INTERNATIONAL JOURNAL OF HYDROGEN ENERGY 43 (2018) 23397–23408

Available online at www.sciencedirect.com

ScienceDirect

journal homepage: www.elsevier.com/locate/he

The effect of hydrogen on the electronic, mechanical and phonon properties of $LaMgNi_4$ and its hydrides for hydrogen storage applications

M.B. Baysal [a], G. Surucu [b,c,d], E. Deligoz [a,*], H. Ozısık [a]

[a] Aksaray University, Department of Physics, 68100, Aksaray, Turkey
[b] Ahi Evran University, Department of Electric and Energy, 40100, Kirsehir, Turkey
[c] Middle East Technical University, Department of Physics, 06800, Ankara, Turkey
[d] Gazi University, Photonics Application and Research Center, 06500, Ankara, Turkey

ARTICLE INFO

Article history:
Received 7 August 2018
Received in revised form
16 October 2018
Accepted 24 October 2018
Available online 16 November 2018

Keywords:
Hydrides
Phonons
Mechanical properties
Elastic properties
Hydrogen storage

ABSTRACT

Density functional theory calculations are used herein to explore the effect of hydrogen on the electronic, mechanical and phonon properties of $LaMgNi_4$ and its hydrides. The polycrystalline elastic moduli, Poisson's ratios and Debye temperatures are calculated based on the single-crystal elastic constants and Voigt-Reuss-Hill approximations. It is also found that all these materials are metallic behavior, ductile and anisotropic in nature. The mechanical anisotropy is discussed via several anisotropy indices and three-dimensional (3D) surface constructions. The effect of high temperature on the free energy, entropy, and heat capacity are also studied by using the quasi-harmonic Debye model. $LaMgNi_4$ and its hydrides are found to be energetically, mechanically and dynamically stable. Also, they are thermodynamically stable and the order of phase stability is $LaMgNi_4H_7$ > $LaMgNi_4H_4$ > $LaMgNi_4H$ > $LaMgNi_4$. In addition, the highest gravimetric hydrogen storage capacity is found to be 1.74 wt% for $LaMgNi4H_7$.

Introduction

Hydrogen, the simplest and most abundant element in the Universe, is widely recognized as a potential energy carrier in a future sustainable and reliable energy system [1]. However, development of safe, compact, robust, and efficient means of hydrogen storage is a major challenge in the realization of a future hydrogen-based energy system. Development of hydrogen storage materials is the key to solving problems with hydrogen storage technology for hydrogen application. Recent studies have mainly focused on innovation and development of hydrogen storage materials such as metal complex hydrides [2]. Magnesium-based alloys are promising candidates for hydrogen storage materials [3–9].

They received much attention during the past decade as cost-efficient hydrogen storage materials allowing the combination of high gravimetric storage capacity of hydrogen with fast rates of hydrogen uptake and release and pronounced destabilization of the metal–hydrogen bonding in comparison with binary Mg–H systems. On the other hand, there are some drawbacks of Mg–H as a hydrogen store such as; hydrogen discharge at high temperature, slow desorption kinetics and a high reactivity toward air and oxygen [10].

* *Corresponding author*. Tel.: +90 382 288 2136.
E-mail address: edeligoz@yahoo.com (E. Deligoz).
https://doi.org/10.1016/j.ijhydene.2018.10.183

Recently, experimental investigations showed that the Mg–Ni–La alloy have suitable temperature range for hydrogen storage and lower dehydrogenization temperature [11], especially rapid dehydrogenization in air by the formation of catalytic water [5]. Also, dual-tuning effect of Indium on the thermodynamic and kinetic properties of Mg_2Ni dehydrogenation is experimentally studied in the literature [12]. $LaMgNi_4$ compound has been synthesized by Kadir et al. [13]. They have also determined the crystal structure for $LaMgNi_4$ by Guinier–Hagg X-ray powder diffraction. According to this work, $LaMgNi_4$ have a cubic $AuBe_5$ type structure with space group F-43m (No. 216). The structural stability, elastic and electronic properties for this compound have been investigated by Wang et al. [14] using first-principles calculations within the generalized gradient approximation. They have reported that $LaMgNi_4$ have strong structural stability. Young et al. [15] have explained combining the XRD, SEM, and TEM studies that the disappearance of the crystalline $LaMgNi_4$ peaks in the XRD pattern is due to a hydrogen-induced amorphization process. Cheng et al. [16] have studied crystal structures, electronic structures and the thermodynamic properties of the $LaMgNi_4$ compound and its hydrides with the density functional theory. Recently, effect of elemental substitution on the structure and hydrogen storage properties of $LaMgNi_4$ alloy have been investigated by Yang et al. [17].

So far, however, some mechanical properties, elastic anisotropy and especially lattice dynamical properties of $LaMgNi_4$ and its hydrides have not been investigated, which is significant for their practical applications. Based on the above reasons, herein, we use DFT calculations to investigate the mechanical, elastic anisotropy, lattice dynamical properties for these compounds. The main goal of this work is to investigate the effect of hydrogen on the mechanical and phonon properties of cubic $LaMgNi_4$, $LaMgNi_4H$, $LaMgNi_4H_7$ and orthorhombic $LaMgNi_4H_4$.

Methodology

The Vienna ab initio simulation package (VASP) [18–20] is used to perform DFT calculations within the generalized gradient approximation of Perdew, Burke, and Ernzerhof (GGA-PBE) [21]. The electron-ion interaction is described under the Projector-augmented wave (PAW) method [22]. The plane wave based pseudo-potential method has been used for the total energy calculations. The valence electronic configuration of La, Mg, Ni, and H are set to [Kr] $4d^1$, [Ne] $3s^2$, [Ar] $3d^84s^2$, $1s^2$, respectively. The energy cut off for the plane wave basis set was fixed at 400 eV. The special k-point sampling of the Brillouin zone (BZ) was employed by using the Monkhorst-Pack method [22] with special $9 \times 9 \times 9$ for $LaMgNi_4$, $LaMgNi_4H$, $LaMgNi_4H_7$ and $8 \times 8 \times 6$ for $LaMgNi_4H_4$ grid points in the primitive cell. In order to determine the ground state geometries for all compounds, the conjugate gradient algorithm with force convergence less than 10^{-7} eV $Å^{-1}$ was used by minimizing stresses and Hellman–Feynman forces. The energy tolerance was less than 10^{-9} eV per unit cell in the iterative solution of the Kohn–Sham equations.

The elastic properties of related compounds were calculated using an efficient stress-strain method [20] implemented in VASP code. The phonon frequencies are calculated using a supercell approach in the PHONOPY code [23] employing the minimum forces on the atoms obtained after geometry optimization. $2 \times 2 \times 2$ supercell for cubic $LaMgNi_4$ (48 atoms), $LaMgNi_4H$ (56 atoms), $LaMgNi_4H_7$ (104 atoms), and for orthorhombic $LaMgNi_4H_4$ (160 atoms) have been used for the phonon calculations.

Results and discussion

Crystal structures and hydrogen storage properties

In order to investigate the ground state physical properties of cubic $LaMgNi_4$, $LaMgNi_4H$, $LaMgNi_4H_7$ and orthorhombic $LaMgNi_4H_4$, the geometry optimizations were performed. Crystal structural for related compounds are demonstrated in Fig. 1. The optimized lattice parameters and volumes are tabulated in Table 1 along with the available theoretical [8,11] and experimental data [5] for comparison, which show that the calculated results are very close to the experimental results.

To determine the relative phase stability of $LaMgNi_4$ and its hydrides, the formation energies have been obtained. The results are given also in Table 1. It is known that negative formation energy usually means an exothermic process and a more negative formation energy corresponds to a better phase stability [25,26]. We have found that formation energies for all the studied materials are negative, see Table 1. This means that $LaMgNi_4$ and its hydrides are stable, $LaMgNi_4H_7$ has the best stability in the four compounds. It can be concluded that phase stability follows the order: $LaMgNi_4H_7$ > $LaMgNi_4H_4$ > $LaMgNi_4H$ > $LaMgNi_4$. More importantly, it is found that, the insertion of hydrogen into the $LaMgNi_4$ compound causes an increase in the phase stability.

The gravimetric hydrogen storage capacity must be considered for $LaMgNi_4$ hydrides. It is the amount of hydrogen stored per unit mass of a material and can be calculated using Equation (1) where H/M is the hydrogen to material atom ratio, M_{Host} is the molar mass of the host material and M_H is the molar mass of hydrogen.

$$C_{wt\%} = \left(\frac{\left(\frac{H}{M}\right) M_H}{M_{Host} + \left(\frac{H}{M}\right) M_H} \times 100 \right)\% \quad (1)$$

The calculated gravimetric hydrogen storage capacities are 0.25 wt% for $LaMgNi_4H$, 1.00 wt% for $LaMgNi_4H_4$ and 1.74 wt% for $LaMgNi_4H_7$. This value is lower than hydrogen storage capacity of $LaMg_2Ni$ (1.96 wt%.) [27] alloy.

The maximum storage capacity among $LaMgNi_4$ hydrides belongs to $LaMgNi_4H_7$ compound.

Electronic properties

The band structures for $LaMgNi_4$ and its hydrides are predicted along the high symmetry directions in the first Brillouin zone from the calculated equilibrium lattice constant. The band structures and corresponding partial and total electronic density of state (DOS) are displayed for $LaMgNi_4$ in Fig. 2 only to save space in the journal. Additionally, the total

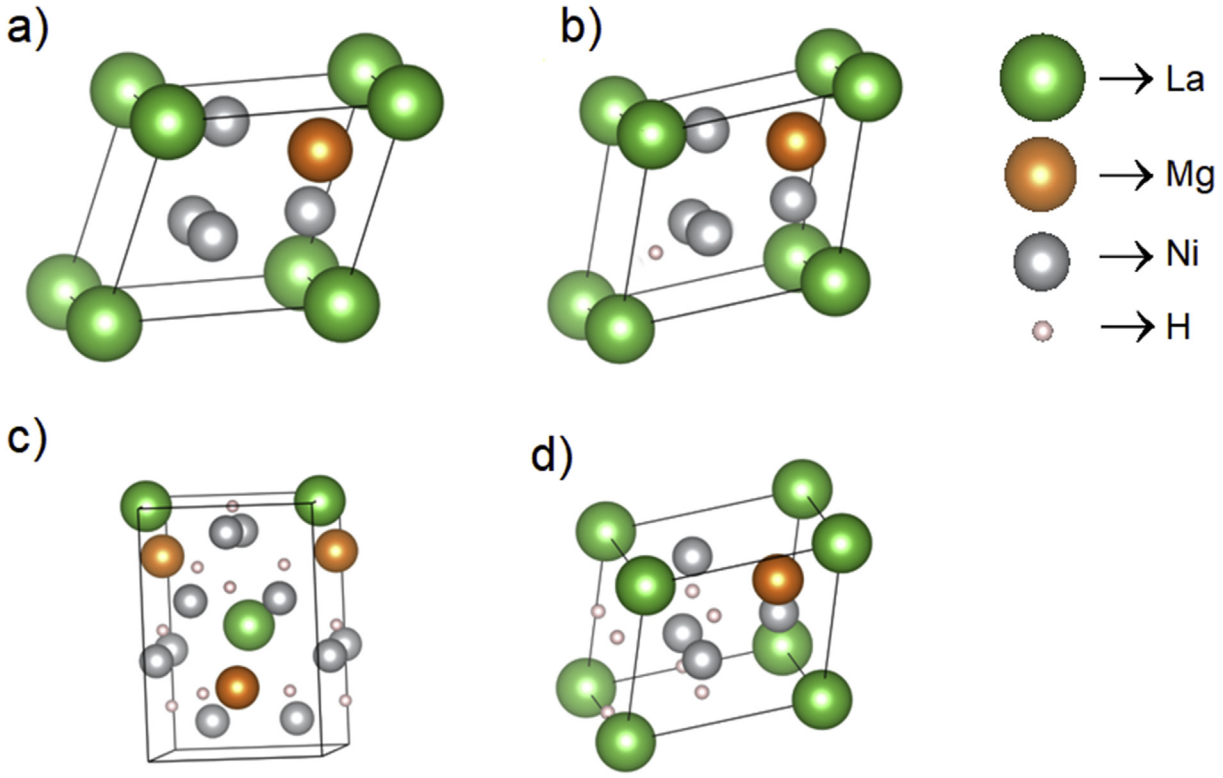

Fig. 1 – 3D crystallographic shapes of $LaMgNi_4$, $LaMgNi_4H$, $LaMgNi_4H_4$ and $LaMgNi_4H_7$ compounds.

Table 1 – Calculated lattice constants (Å), volume ($Å^3$/f.u.), formation energy (eV/atom), W_{occ} (width of occupied states)/W_b (bonding states) ratio, and electron numbers at Fermi level (n) for $LaMgNi_4$, $LaMgNi_4H$, $LaMgNi_4H_4$ and $LaMgNi_4H_7$ compounds with the other results from the literature.

Compounds	a	b	c	V	ΔH	W_{occ}/W_b	n	Reference
$LaMgNi_4$	7.13			90.94	−0.30	1.12	4.20	This study
	7.15			91.6	−0.33			Theory*
	7.55							Theory**
	7.17			92.15				Experiment***
$LaMgNi_4H$	7.25			95.57	−0.62	0.93	16.81	This study
	7.98							Theory**
	7.27			96.06				Experiment***
$LaMgNi_4H_4$	5.10	5.52	7.39	104.24	−1.15	0.96	8.36	This study
	5.82	5.56	7.99					Theory**
	5.12	5.52	7.45	105.27				Experiment***
$LaMgNi_4H_7$	7.72			115.20	−1.40	0.98	3.62	This study
	7.96							Theory**
	7.65			111.92				Experiment***

Reference *[8], **[11], ***[5].

DOS for $LaMgNi_4$ and its hydrides due to the atoms are given in Fig. 3. As seen from the figure, the DOS values vary from zero at the Fermi level which indicates that all compounds are metallic. The variation of electron numbers at Fermi levels are given in Table 1. Having the lowest electron number demonstrates the most stability structure which is also consistent with the estimation from formation enthalpy of $LaMgNi_4H_7$ (n = 3.62).

Moreover, the structural phase stability of a crystal can be examined from the plotted DOS curves by using band filling theory [28–30]. According to the theory, the phase stability of a crystal depends upon the band filling of the bonding states and the width of the occupied states (W_{occ}) can be calculated as the distance from the bottom of the band to Fermi level (E_F). Also, the width of the bonding states (W_b) can be calculated as the distance from the bottom of the band to E_F and to the pseudogap, respectively. Then, W_{occ}/W_b ratio may give well information about the phase stability of a material. The stability increases while this ratio is close to 1, otherwise the stability decreases. In this work, the obtained W_{occ}/W_b ratios of these compounds much close to 1 which shows that, these materials are structurally stable, as seen in Table 1. In addition, electron numbers at Fermi level (n) of $LaMgNi_4H_7$ is the lowest value and so, the phase stability of this material is

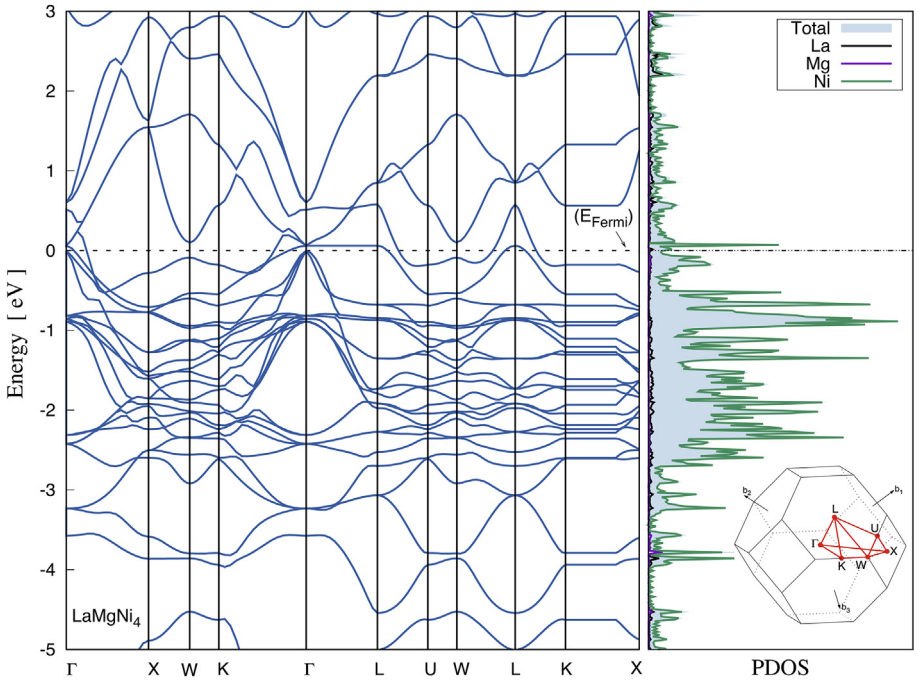

Fig. 2 – Calculated the electronic band structure and the corresponding total density of states and partial density of states of the $LaMgNi_4$ compound.

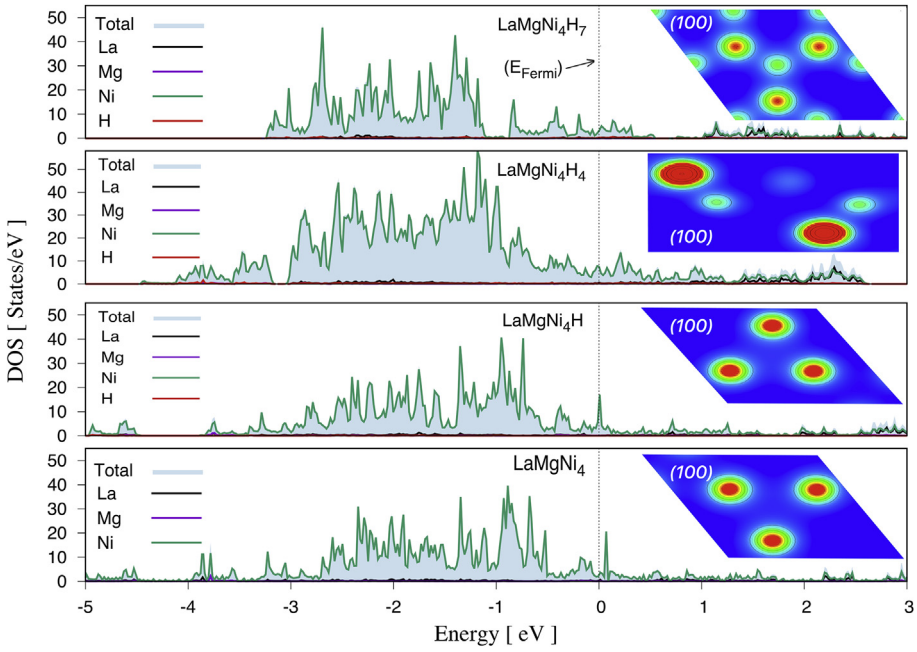

Fig. 3 – Calculated total density of states and partial density of states of $LaMgNi_4$, $LaMgNi_4H$, $LaMgNi_4H_4$ and $LaMgNi_4H_7$ compounds.

higher than the others. In addition, the valence charge density is calculated to visualize the nature of the bonding character for $LaMgNi_4$ and its hydrides. The charge density plots have been inserted in Fig. 3. $LaMgNi_4$ and its hydrides have ionic bonding that are also consistent with Poisson's ratios of the compounds.

The Bader partial charge analysis provides to obtain the charges of each ion in the structure. The positive Bader net charge means that the charge is transferred away from the ion and the charge is transferred to the ion if the Bader net charge is negative [26,31]. The Bader partial charge has been calculated using VASP for $LaMgNi_4$ hydrides and the algorithm developed by Henkelman group [32] is performed for analysis of VASP result. The total Bader net charges are given in Table 2 for $LaMgNi_4$ hydrides. If the crystal structures are different, then the number of La, Mg and Ni atoms are different.

Table 2 – Bader net charge of the atoms for $LaMgNi_4H_x$ in units of e.

	La (+11)	Mg (+2)	Ni (+10)	H (+1)
$LaMgNi_4$	−4.511	−6.322	10.833	
$LaMgNi_4H$	−2.712	−7.843	11.294	−0.739
$LaMgNi_4H_4$	2.581	−7.702	25.260	−20.139
$LaMgNi_4H_7$	−1.106	−2.315	20.974	−17.553

Therefore, Bader net charge for the same atom in various structures are changing. The charge is transferred to La and Mg atoms and it is transferred away from Ni atoms for $LaMgNi_4$ compound as can be seen from Table 2. For $LaMgNi_4H$ and $LaMgNi_4H_7$ compounds, H atoms get charge from Ni atoms. However, H atoms get charge from Ni and La atoms in the $LaMgNi_4H_4$ compound. In addition, net Bader charge of H atoms increases from $LaMgNi_4H$ to $LaMgNi_4H_7$ that indicates more strong bonds in the compounds. $LaMgNi_4H$ compounds could easily release H though having low storage capacity among the studied compounds due to having weak bonds between H and Ni atoms.

Mechanical properties

The independent elastic constants (C_{11}, C_{12} *and* C_{44} for cubic structure, C_{11}, C_{22}, C_{33}, C_{44}, C_{55}, C_{66}, C_{12}, C_{13}, and C_{23} for orthorhombic structure) at 0 GPa and 0 K are successfully obtained by the stress and strain method. The results are listed in Table 3. The obtained elastic constant for $LaMgNi_4$ are in well agreement with the theoretical data. No experiments have been conducted out to measure the single crystal elastic constants C_{ij} for the other compounds to be compared with our obtained results. Therefore, the present results could provide useful information for further experimental or theoretical investigations.

For the stable structures, these elastic constants should satisfy the Born stability criteria [27,33].

For cubic structure:

$$C_{11}>0,\ C_{44}>0,\ C_{11}>C_{12},\ \text{and}\ C_{11}+2C_{12}>0$$

For the orthorhombic structure:

$$C_{11}>0,\ C_{22}>0,\ C_{33}>0,\ C_{44}>0,\ C_{55}>0,\ C_{66}>0$$

$$[C_{11}+C_{22}+C_{33}+2(C_{12}+C_{13}+C_{23})]>0$$

$$(C_{11}+C_{22}-2C_{12})>0,\quad (C_{11}+C_{33}-2C_{13})>0,$$

$$(C_{22}+C_{33}-2C_{23})>0$$

The calculated elastic constants C_{ij} (see Table 3) satisfy the Born stability criteria. Thus, the $LaMgNi_4$ and its hydrides is mechanically stable at ambient pressure. $LaMgNi_4H_4$ has the highest C_{11}, which shows that this compound has high incompressibility under uniaxial stress along a-axis. On the other hand, elastic constant C_{44} reflects the resistance to shear in (010) or (100) planes in the [001] direction [34]. $LaMgNi_4H_4$ have largest C_{44} among these compounds, indicating that $LaMgNi_4H_4$ exhibits higher resistance along these directions. In $LaMgNi_4$ and its hydrides, $C_{11} > C_{44}$ suggest that [100] (100) shear is easier than [100] (010) shear. Moreover, the calculated C_{22} and C_{33} are the relatively same and C_{11} is larger than them for orthorhombic $LaMgNi_4H_4$. This implies that the atomic bonding between nearest neighbors along the (010) and (001) planes have the same strength, different from that of (100) plane. It implies that the compound shows less compressibility along c axis compared to the two others. Besides, the interatomic forces in the stannate pyrochlores are not centrosymmetric because we found that $C_{11} \neq C_{44}$ for all compounds, and thus we conclude that the mechanical properties of the compounds are direction-dependent [35].

From the single-crystal elastic constants, one can calculate other important elastic moduli through the following equations [36,37]:

For the cubic structure:

$$G_v = (C_{11} - C_{12} + 3C_{44})/5 \tag{2}$$

$$G_R = 5\,C_{11} - C_{12} - C_{44}/[4C_{44} + 3\,C_{11} - C_{12}] \tag{3}$$

$$B_V = B_R = (C_{11} + 2C_{12}) \tag{4}$$

On the other hand.

For the orthorhombic structure:

$$B_v = (1/9)[C_{11} + C_{22} + C_{33} + 2(C_{12} + C_{13} + C_{23})] \tag{5}$$

$$B_R = \Delta \begin{bmatrix} C_{11}(C_{22}+C_{33}-2C_{23}) + C_{22}(C_{33}-2C_{13}) - 2C_{33}C_{12} + \\ C_{12}(2C_{23}-C_{12}) + C_{13}(2C_{12}-C_{13}) + C_{23}(2C_{13}-C_{23} \end{bmatrix}^{-1} \tag{6}$$

$$\Delta = C_{13}(C_{12}C_{23} - C_{13}C_{22}) + C_{23}(C_{12}C_{13} - C_{23}C_{11}) + C_{33}\left(C_{11}C_{22} - C_{12}^2\right) \tag{7}$$

$$G_V = (1/15)[C_{11} + C_{22} + C_{33}2(C_{12} + C_{13} + C_{23})] \tag{8}$$

Table 3 – Calculated elastic constants (C_{ij}, GPa) for $LaMgNi_4$, $LaMgNi_4H$, $LaMgNi_4H_4$ and $LaMgNi_4H_7$ compounds with the other results from the literature.

Compounds	C_{11}	C_{12}	C_{13}	C_{22}	C_{23}	C_{33}	C_{44}	C_{55}	C_{66}	Reference
$LaMgNi_4$	153.6	88.6					47.7			This study
	154.9	88.0					48.6			Theory*
$LaMgNi_4H$	161.2	86.1					32.7			This study
$LaMgNi_4H_4$	181.1	71.0	78.6	159.5	93.0	157.2	53.2	50.8	35.3	This study
$LaMgNi_4H_7$	149.8	89.6					34.5			This study

Reference *[8].

$$G_R = 15\left\{4\left[\begin{matrix}C_{11}(C_{22}+C_{33}+C_{23})+C_{22}(C_{33}+C_{13})-C_{33}C_{12}-\\ C_{12}(C_{23}-C_{12})-C_{13}(C_{12}+C_{13})-C_{23}(C_{13}+C_{23})\end{matrix}\right]\Big/\Delta+3[(1/C_{44})+(1/C_{55})+(1/C_{66})]\right\}^{-1} \quad (9)$$

$$\Delta = C_{13}(C_{12}C_{23}-C_{13}C_{22})+C_{23}(C_{12}C_{13}-C_{23}C_{11})+C_{33}(C_{11}C_{22}-C_{12}^2) \quad (10)$$

The elastic moduli can be approximated by the Hill's average [38] as the following

$$B = \frac{B_R + B_V}{2} \quad (11)$$

$$G = \frac{G_R + G_V}{2} \quad (12)$$

Young's modulus (E) and Poisson's ratio (ϑ) are given by the following equations:

$$E = \frac{9GB}{G+3B} \quad (13)$$

$$\vartheta = \frac{3B-2G}{2(3B+G)} \quad (14)$$

The results are summarized in Table 4 together with available theoretical value for $LaMgNi_4$. Table 4 shows that the obtained bulk modulus for all materials are close to each other with small differences. Hence, we conclude that $LaMgNi_4$ and its hydrides have almost same volume change with pressure. Moreover, cubic $LaMgNi_4H$ and $LaMgNi_4H_7$ show lower shear and Young's modulus than $LaMgNi_4$ while orthorhombic $LaMgNi_4H_4$ shows higher shear and Young's modulus than $LaMgNi_4$. Orthorhombic $LaMgNi_4H_4$ also has the largest Young's modulus, implying it is the stiffest material. It is worth to note here that the bulk modulus for all compounds is three times the shear modulus value, indicating that the shear deformation is easier to occur compared to the compressional deformation.

Poisson's ratio can be used to determine the bonding nature of the solids. If a solid is covalent bound the v value is 0.1, for metallic solids the v value is 0.33 [39]. From Table 4, we can see that the values of these compounds are between 0.32 and 0.36, showing that these compounds have metallic bonding in considered structures. It can be noted that the Poisson's ratio for cubic structure increase with the hydrogen content increasing in $LaMgNi_4$. Consequently, in cubic structure, the absorption of H improves the plasticity [40].

The brittleness and ductility of the material are related to the value of B/G and Poisson's ratio ν. According to Pugh's criterion [39], a high (low) B/G value is correlated with the ductility (brittleness) of the material. The critical value of the ductile-to-brittle transition was observed to be ~1.75. The obtained B/G ratios are higher than 1.75, indicating the ductility nature of all compounds. In addition to that, the ratio of B/G increases with the number of H atoms inserted in $LaMgNi_4$ except for $LaMgNi_4H_4$, indicating that the concentration of H atoms can change the ductility. The similar results have been observed by Benyelloul et al. [40].

Frantsevich et al. [41] have distinguished the ductility/brittleness of the materials in terms of Poisson's ratio. Generally, the ductility material has a higher Poisson's ratio than 0.26. According to this criterion, all the herein considered compounds can be classified as ductility materials, which are consistent with the B/G ratios for $LaMgNi_4$ and its hydrides.

The Debye temperature (θ_D) is related to many parameters such as melting point, thermal expansion coefficient, and specific heat. The Debye temperature is obtained using the following well known equations [42]:

$$\theta_D = \frac{h}{k}\left[\frac{3n}{4\pi}\frac{N_A\rho}{M}\right]^{1/3} v_m \quad (15)$$

here, h is the Planck's constant, k is the Boltzmann's constant, n is the number of atoms per formula unit, ρ is the mass density, and M is the mass of atoms contained in the unitcell, N_A is the Avogadro number.

The average sound velocity (ν_m), the longitudinal (ν_l) and transverse (ν_t) sound velocities are given as [43,44]:

$$v_m = \left[\frac{1}{3}\left(\frac{2}{v_t^3}+\frac{1}{v_l^3}\right)\right]^{-1/3} \quad (16)$$

$$v_t = \sqrt{\frac{G}{\rho}} \quad (17)$$

Table 4 – Calculated bulk modulus (B, GPa), shear modulus (G, GPa), Young's modulus (E, GPa), B/G ratio, Poisson's ratio (ν), hardness (H, GPa). Debye temperature (θ_D, Kelvin), longitudinal sound velocity (ϑ_l, *m/s*), transverse sound velocity (ϑ_t, *m/s*), average sound velocity (ϑ_m, *m/s*) for $LaMgNi_4$, $LaMgNi_4H$, $LaMgNi_4H_4$ and $LaMgNi_4H_7$ compounds with the other results from the literature.

Compounds	B	G	E	B/G	ν	H_V	θ_D	ϑ_l	ϑ_t	ϑ_m	Reference
$LaMgNi_4$	110.2	40.8	108.9	2.70	0.33	2.47	351.5	4929	2615	2922	This study
	110.3	38.9	104.4		0.34						Theory*
$LaMgNi_4H$	111.1	34.5	93.7	3.22	0.35	1.03	392.2	5170	2824	3149	This study
$LaMgNi_4H_4$	109.2	43.8	115.9	2.49	0.32	3.24	399.3	5117	2616	2930	This study
$LaMgNi_4H_7$	109.6	32.6	88.9	3.36	0.36	0.60	452.6	5528	2807	3146	This study

Reference *[8].

Table 5 – Calculated anisotropic factors A_1, A_2, A_3, A_B, A_G (percent elastic anisotropy in compression and shear) and A^U (universal anisotropic index) for $LaMgNi_4$, $LaMgNi_4H$, $LaMgNi_4H_4$ and $LaMgNi_4H_7$ compounds with the other results from the literature.

Compounds	A_1	A_2	A_3	A_B	A_G	A^U	Reference
$LaMgNi_4$	1.468	1.468	1.468	0	1.836	0.178	This study
	1.196	1.196	1.196				Theory*
$LaMgNi_4H$	0.871	0.871	0.871	0	0.290	0.022	This study
$LaMgNi_4H_4$	1.175	1.555	0.711	0.017	2.310	0.235	This study
$LaMgNi_4H_7$	1.146	1.146	1.146	0	0.310	0.022	This study

Reference *[8].

$$v_l = \sqrt{\frac{3B + 4G}{3\rho}} \tag{18}$$

The calculated Debye temperature and sound velocities are also, shown in Table 4. The order of θ_D for these compounds is $LaMgNi_4H_7$ > $LaMgNi_4H_4$ >$LaMgNi_4H$ > $LaMgNi_4$. This can suggest that the Debye temperature increase gradually with increasing number of H atoms, indicating that $LaMgNi_4$ compound has stronger bonds when inserting H atoms.

Elastic anisotropy

Elastically anisotropic parameters have an important implication in engineering science. The elastic anisotropy can be characterized by the Zener anisotropic factors (A_1, A_2 and A_3) and by the indexes describing the behavior in shear and compression (A_G and A_B) [45]. These parameters had been proposed as follows [45].

For cubic structure

$$A_1 = A_2 = A_3 = 2C_{44}/C_{11} - C_{12} \tag{19}$$

For orthorhombic structure.

For the {1 0 0} shear plane is defined as:

$$A_1 = \frac{4C_{44}}{(C_{11} + C_{33} - 2C_{13})} \tag{20}$$

For the {010} shear plane it is:

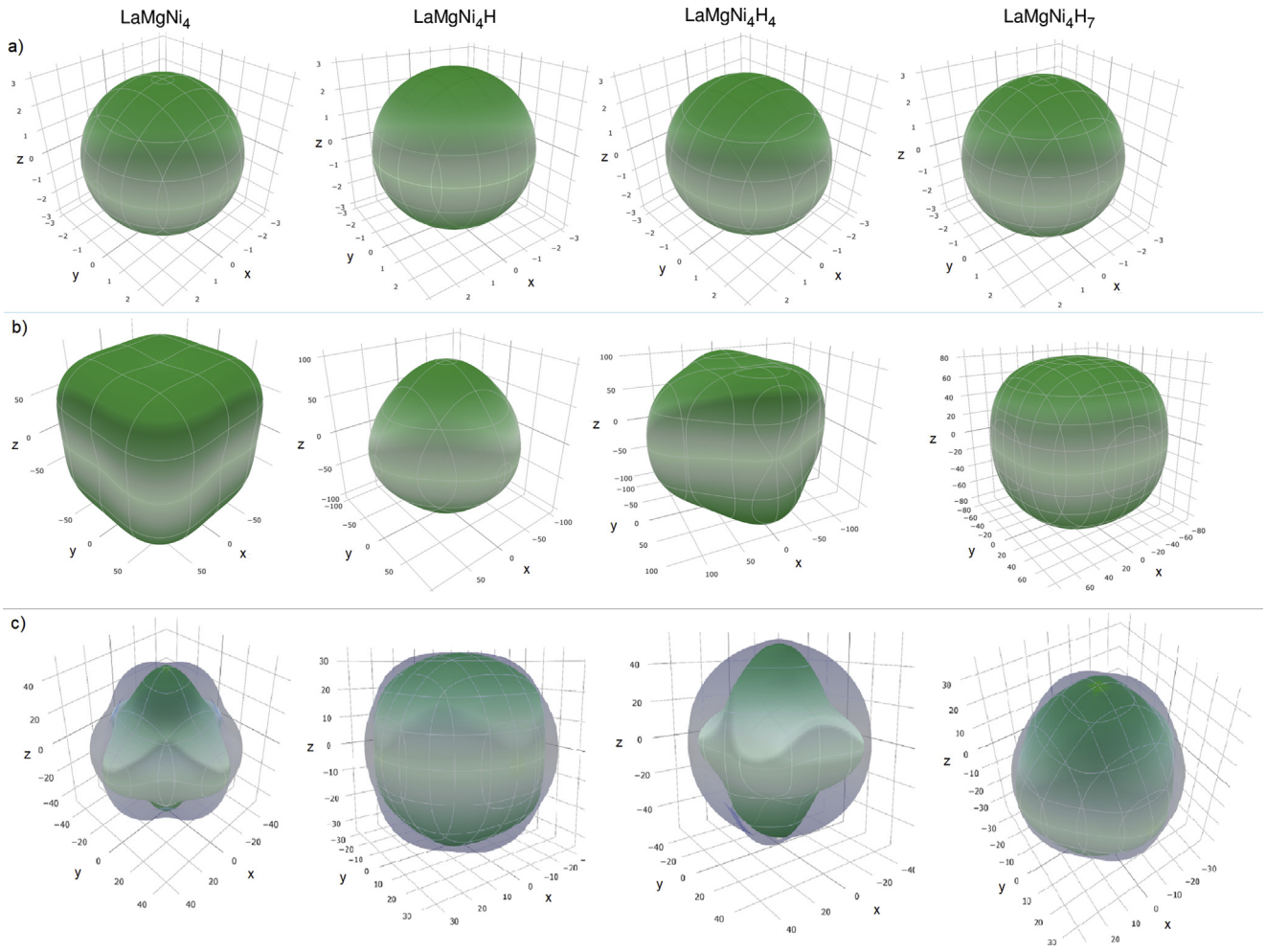

Fig. 4 – 3D directional dependence of (*a*) the compressibility (in TPa^{-1}), (*b*) Young's modulus (in GPa), and (*c*) Shear modulus (in GPa) for $LaMgNi_4$, $LaMgNi_4H$, $LaMgNi_4H_4$ and $LaMgNi_4H_7$ compounds.

$$A_2 = \frac{4C_{55}}{(C_{22} + C_{33} - 2C_{23})} \quad (21)$$

and for the {001} shear plane it is:

$$A_3 = \frac{4C_{66}}{(C_{11} + C_{22} - 2C_{12})} \quad (22)$$

$$A_G = \frac{G_v - G_R}{G_v + G_R} x100 \quad (23)$$

$$A_B = \frac{B_v - B_R}{B_v + B_R} x100 \quad (24)$$

Both A1, A_2 and A_3 must be equal to one for an isotropy crystal, while any value smaller or greater than one measures the degree of elastic anisotropy. Otherwise, it is anisotropic. $A_B = A_G = 0$ means the elastic isotropy, whereas $A_B = A_G = 1$ refers the maximum elastic anisotropy [46].

On the other hand, the universal elastic anisotropy is also considered to describe the elastic anisotropy, which are defined as [47].

$$A^u = 5\frac{G_v}{G_R} + \frac{B_v}{B_R} - 6 \quad (25)$$

It is known that the universal elastic anisotropy index A^U is equal to zero, namely the crystal with $A^U = 0$ is elastically isotropic. The calculated elastically anisotropic parameters are given in Table 5. The values of A^U of these compounds indicate that $LaMgNi_4H_4$ has the most highly elastic anisotropy according to the A^U value of 0.235. As for the shear anisotropic factors, their values are larger or smaller than unity, which indicates the shear anisotropy of these compounds. Besides, we have observed that the predicted Zener anisotropic factor of $LaMgNi_4H_4$ is maximal for the {010} shear plane. A listed in Table 5 clearly show that $LaMgNi_4$ and its hydrides are elastically anisotropic.

The above elastic anisotropic indexes are not sufficient to characterize the elastic anisotropy. Therefore, the EIAM code [48] has been used to describe the directional elastic anisotropy of these compounds. We plot the three-dimensional curved surface of linear compressibility, Young's modulus and shear modulus. The deviation degree from the spherical surface indicates the content of anisotropy [49].

The 3D figures of three compounds are plot in Fig. 4. For linear compressibility (see In Fig. 4a), the 3D surface of the $LaMgNi_4H_7$, $LaMgNi_4H$ and $LaMgNi_4$ exhibit a noticeable isotropic. The shape of surface of $LaMgNi_4H_4$ is far from the spherical shape and exhibit relatively an anisotropy. According to Fig. 4b and c, Young's modulus and shear modulus possess obvious anisotropy. $LaMgNi_4H_4$ has the most highly elastic anisotropy, while $LaMgNi_4H_7$ possesses the least elastic anisotropy according to these figures. It can be noted that $LaMgNi_4H_4$ are clearly exhibits anisotropic behavior in x planes, while It relatively isotropic in y and z planes. The reason is that the calculated elastic constant C_{11} is higher than C_{22}, C_{33} and, the values of C_{22} and C_{33} are close to each other with small differences. The present results are consistent with the conclusion from the analysis of index A^u, A_G, A_B, A_1, A_2, and A_3.

Lattice dynamical properties

Phonon calculations can provide information regarding dynamical stability and vibrational contribution for a crystal. In context to, the obtained phonon dispersion curves and corresponding phonon density of states (PHDOS) for $LaMgNi_4$ and its hydrides by using the linear response approach are plotted in Figs. 5–8. It is clearly seen that the phonon

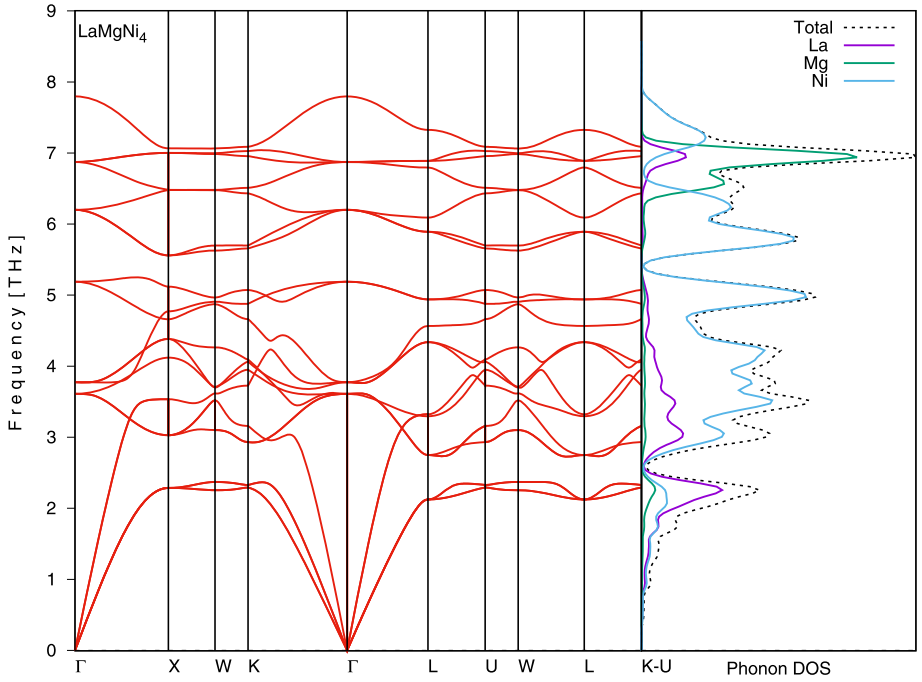

Fig. 5 – The phonon dispersions and corresponding density of states for $LaMgNi_4$ compound.

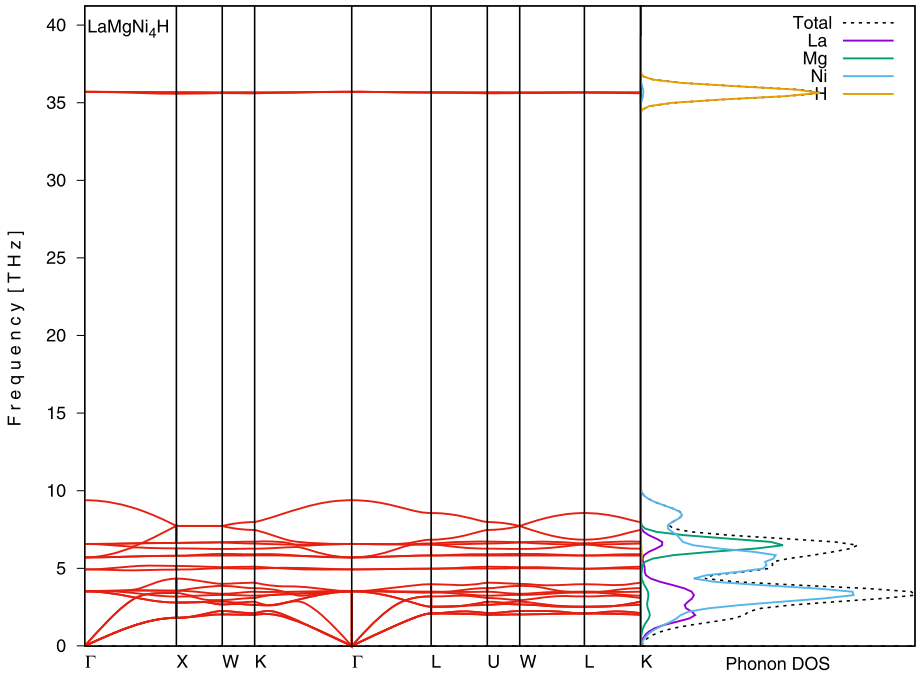

Fig. 6 – The phonon dispersions and corresponding density of states for $LaMgNi_4H$ compound.

dispersion spectrum has no imaginary frequencies, indicating the dynamical stability of $LaMgNi_4$ and its hydrides. The unit cell of $LaMgNi_4$, $LaMgNi_4H$, $LaMgNi_4H_4$, and $LaMgNi_4H_7$ contain 6, 7, 20 and 13 atoms which gives rise to 18, 21, 60, and 39 phonon branches, respectively. These phonon modes contain 3 acoustic modes and 15, 18, 57, and 36 optical modes for $LaMgNi_4$, $LaMgNi_4H$, $LaMgNi_4H_4$, and $LaMgNi_4H_7$, respectively.

We find that almost all the phonon frequencies are upward with the number of H atoms inserted in $LaMgNi_4$. For these compounds, the optical branches and acoustic branches of phonon curves overlap each other and are not separated by a gap. The highest optical branches are separated from the rest of the phonon branches with the number of H atoms inserted in $LaMgNi_4$. The appearance of optical phonon band gap is attributed to the large mass difference between H atoms and other atoms. On the right side of phonon dispersion curves, PHDOS is also showed for these compounds. The sharp peaks in the PHDOS correspond to the flat modes of the phonon

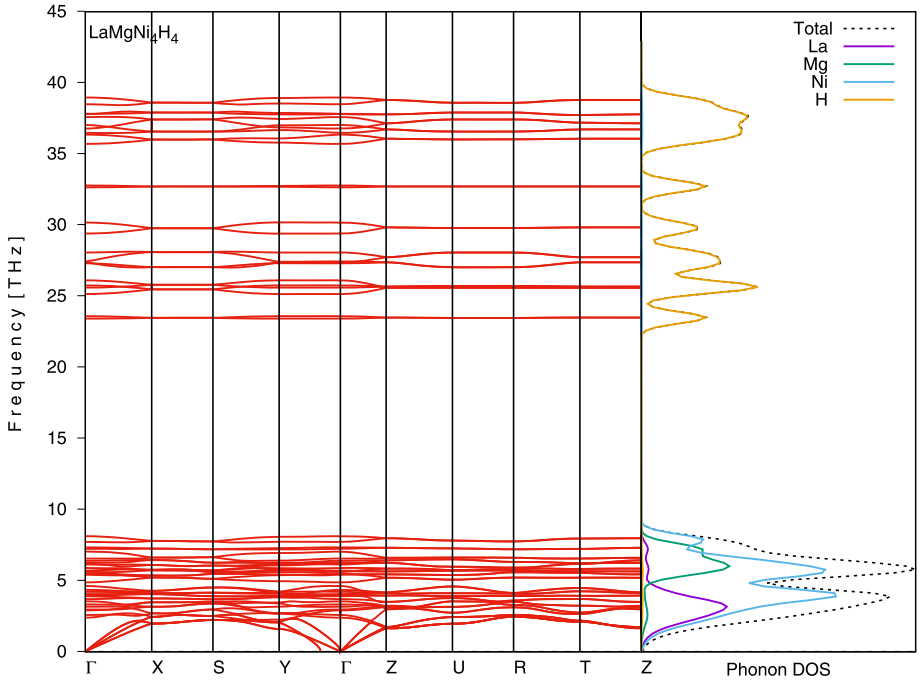

Fig. 7 – The phonon dispersions and corresponding density of states for $LaMgNi_4H_4$ compound.

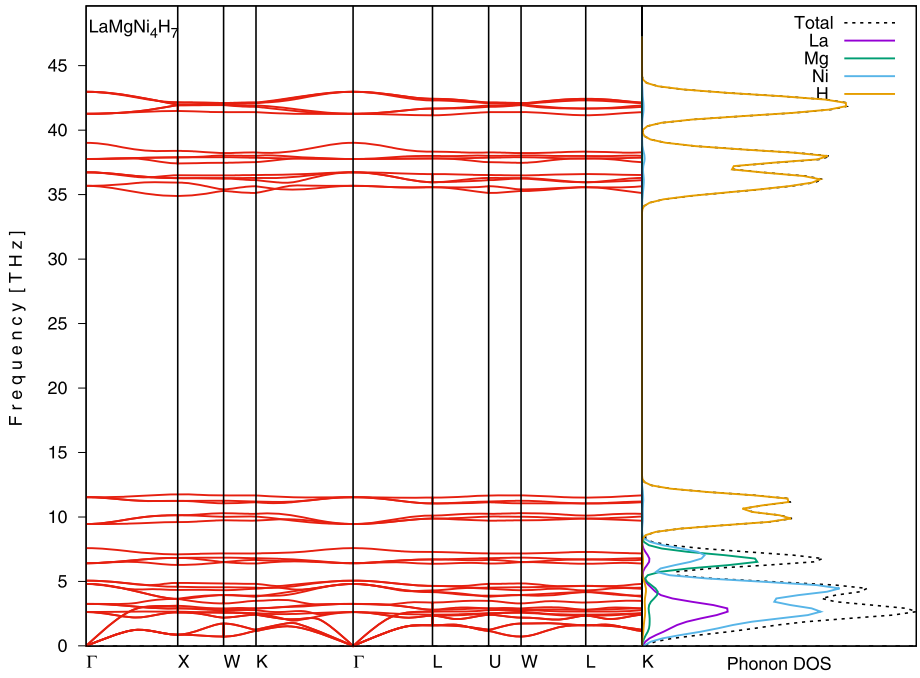

Fig. 8 – The phonon dispersions and corresponding density of states for $LaMgNi_4H_7$ compound.

dispersion curves. The main contribution to acoustic phonons (<3 THz) for all compounds comes from the La atoms, while between about 3 and 7 THz are dominated by the Ni atoms for $LaMgNi_4$ and Ni and Mg atoms for other compounds. The optical modes (>7 THz) for $LaMgNi_4$ are attributed to the vibrations of the Mg atoms while $LaMgNi_4H$, $LaMgNi_4H_4$, and $LaMgNi_4H_7$ containing are motions of the H atoms.

Thermodynamic quantities, such as the Helmholtz free energy (F), entropy (S), constant volume heat capacity (C_V) in the temperature range of 0–2000 K for $LaMgNi_4$ and its hydrides, can be calculated using phonon information and quasi-harmonic approximation [24]. Thermodynamic properties help to evaluate some important features of a material like its behavior under temperature. The results are illustrated in Figs. 9–11 given in units of per atom. It can be seen that such changes with temperature almost a common trend in $LaMgNi_4$ and its hydrides. As one can notice, free energy is nearly constant from 0 to 100 K and decreases linearly with increasing temperature from $T > 100$ K. Inversely, the entropy increases with increasing temperature. It is apparent from Fig. 9 that heat capacity increases. Moreover, the free energy gradually increases while the entropy and heat capacity

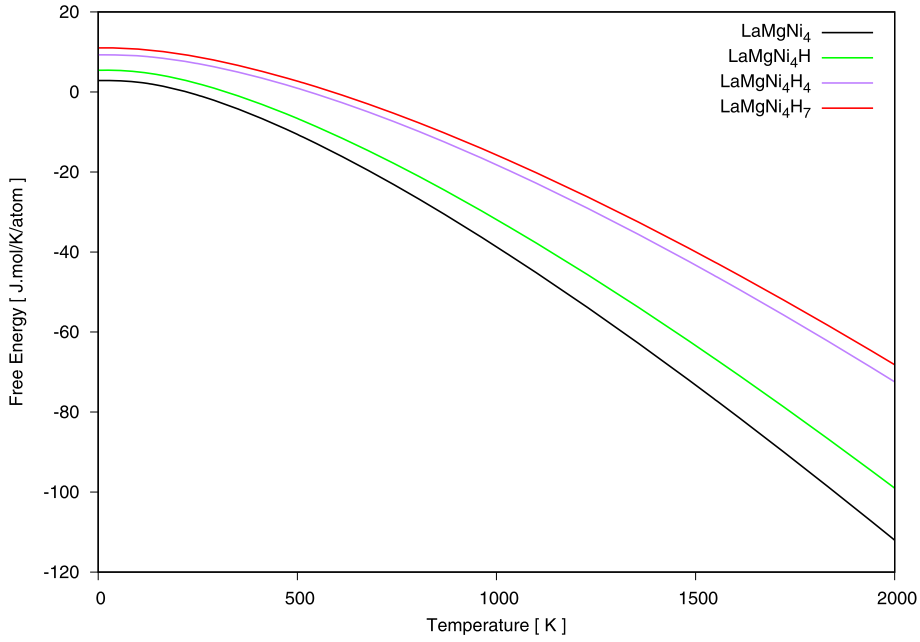

Fig. 9 – The temperature dependence of free energy for $LaMgNi_4$, $LaMgNi_4H$, $LaMgNi_4H_4$ and $LaMgNi_4H_7$ compounds.

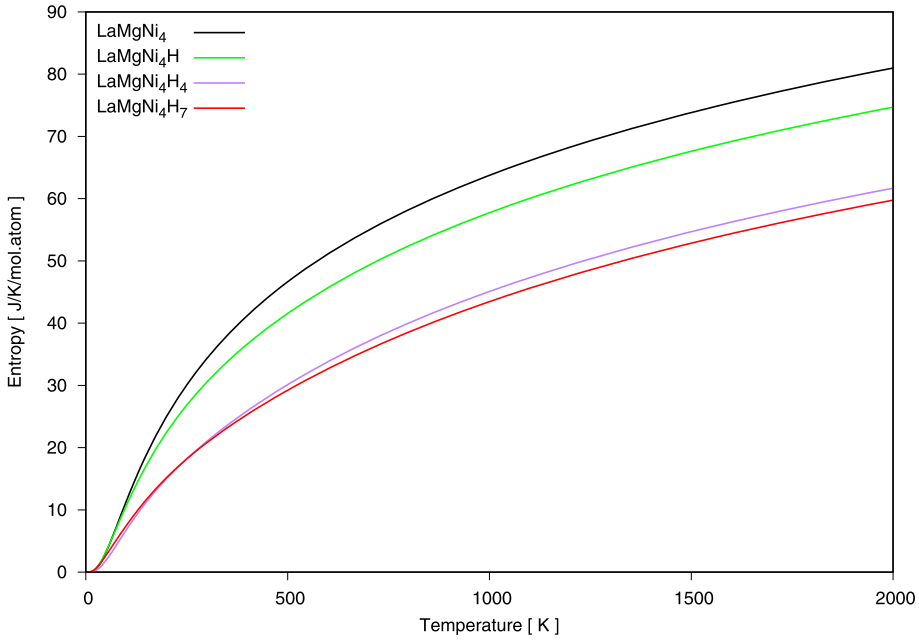

Fig. 10 – The temperature dependence of entropy for $LaMgNi_4$, $LaMgNi_4H$, $LaMgNi_4H_4$ and $LaMgNi_4H_7$ compounds.

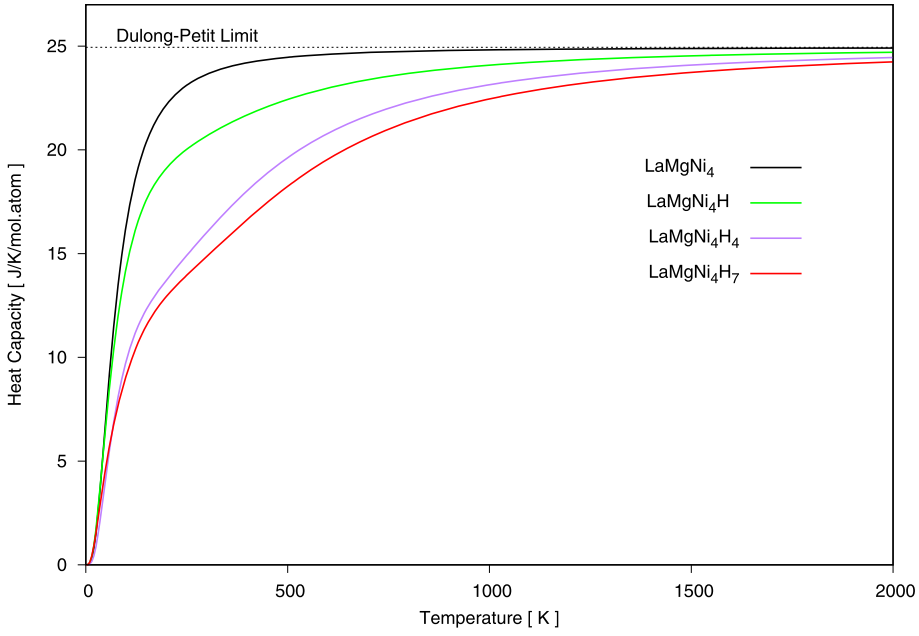

Fig. 11 – The temperature dependence of heat capacity for $LaMgNi_4$, $LaMgNi_4H$, $LaMgNi_4H_4$ and $LaMgNi_4H_7$ compounds.

decrease with the number of H atoms inserted in $LaMgNi_4$. This may be due to the contribution from higher frequencies resulting from lighter H atom vibrations.

Conclusions

The structural parameters, electronic, elastic and lattice dynamical properties for $LaMgNi_4$ and its hydrides are calculated by first-principles calculation within the generalized gradient approximation based on density functional formalism. The obtained negative formation enthalpies suggest that the all compounds are provided with thermodynamically stable crystal structure. The band structures for all compounds are metallic in nature. The obtained DOS and charge density maps show that all compounds dominantly have ionic in nature. From the elastic parameter behavior, it is inferred that these compounds are elastically stable and ductile in nature. The variation of B/G ratio increases with increasing the number of H atoms, indicating that the concentration of H can change the ductility. The calculated elastic anisotropy indexes indicate that the all compounds exhibit

obvious anisotropy. The calculated phonon frequency indicating that all compounds are dynamically stable. Furthermore, almost all the phonon frequencies are upward with the number of H atoms inserted in $LaMgNi_4$. The free energy gradually increases while the entropy and heat capacity decrease with the insertion of hydrogen into the $LaMgNi_4$ compound. In addition, the highest hydrogen storage capacity is obtained for $LaMgNi_4H_7$. Our results are helpful to understand the hydrogen storage mechanism and design new hydrogen storage materials in magnesium-based alloys.

Acknowledgments

In this paper, the numerical calculations reported were partially performed at TUBITAK ULAKBIM High Performance and Grid Computing Center and Aksaray University, Science and Technology Application and Research Center.

REFERENCES

[1] Ravnsbæk DB, Nickels EA, Cerný R, Olesen CH, David WIF, Edwards PP, et al. Inorg Chem 2013;52:10877–85.
[2] Zhang HJ, Xu B, Li X, Zeng Y, Meng L. Int J Hydrogen Energy 2014;39:17144–52.
[3] Güther V, Otto A. J Alloy Comp 1999;293–295:734–6.
[4] Stan C, Andronescu E, Predoi D, Bobet JL. J Alloy Comp 2008;461:228–34.
[5] Guenee L, Favre-Nicolin V, Yvon K. J Alloy Comp 2003;348:129–37.
[6] Ma M, Duan R, Ouyang L, Zhu X, Peng C, Zhu M. Int J Hydrogen Energy 2017;42:22312–7.
[7] Zhu M, Wang H, Ouyang LZ, Zeng MQ. Int J Hydrogen Energy 2006;31:251–7.
[8] Jain IP. Int J Hydrogen Energy 2010;35:5133–44.
[9] Ouyang LZ, Yang XS, Zhu M, Liu JW, Dong HW, Sun DL, et al. J Phys Chem C 2014;118:7808–20.
[10] Sakintuna B, Lamari-Darkrim F, Hirscher M. Int J Hydrogen Energy 2007;32:1121–40.
[11] Aono K, Orimo S, Fujii H. J Alloy Comp 2000;309:L1–4.
[12] Ouyang LZ, Cao ZJ, Wang H, Liu JW, Sun DL, Zhang QA, et al. Int J Hydrogen Energy 2013;38:8881–7.
[13] Kadir K, Noreus D, Yamashita I. J Alloy Comp 2002;345:140–3.
[14] Wang J-W, Yang F, Fan T-W, Tanga B-Y, Peng L-M, Ding W-J. Physica B 2011;406:1330–5.
[15] Young K, Ouchi T, Shen H, Bendersky LA. Int J Hydrogen Energy 2015;40:8941–7.
[16] Cheng LF, Zoua JX, Zenga XQ, Dinga W. J Intermetallics 2013;38:30–5.
[17] Yang T, Yuan Z, Bu W, Jia Z, Qi Y, Zhang Y. Mater Des 2016;93:46–52.
[18] Kresse G, Furthmuller J. Comput Mater Sci 1996;6:15–50.
[19] Blochl PE. Phys Rev B 1994;50:17953–79.
[20] Kresse G, Furthmuller J. Phys Rev B 1996;54:11169–86.
[21] Perdew JP, Burke K, Ernzerhof M. Phys Rev Lett 1996;77:3865–8.
[22] Monkhorst HJ, Pack JD. Phys Rev B 1976;13:5188–92.
[23] Le Page Y, Saxe P. Phys Rev B 2002;65. 104104 1-14.
[24] Togo A, Oba F, Tanaka I. Phys Rev B 2008;78. 134106 1-9.
[25] Gencer A, Surucu G. Mater Res Express 2018;5:076303.
[26] Turkdal N, Deligoz E, Ozisik H, Ozisik HB. Phase Transitions 2017;90(6):598–609.
[27] Ouyang LZ, Yao L, Dong HW, Li LQ, Zhu M. J Alloy Comp 2009;485:507–9.
[28] Xu JH, Freeman AJ. Phys Rev B 1989;40:11927–30.
[29] Xu JH, Oguchi T, Freeman AJ. Phys Rev B 1987;35:6940–3.
[30] Surucu G, Colakoglu K, Deligoz E, Ciftci YO. Solid State Commun 2013;171:1–4.
[31] Pan RK, Yao JG, Ji RL, Liu WW, Yin DF. Int J Hydrogen Energy 2018;43:3862–70.
[32] Henkelman G, Arnaldsson A, Jónsson H. Comput Mater Sci 2006;36:354–60.
[33] Born M. Proc Camb Philos Soc 1940;36:160–72.
[34] He T, Jiang Y, Zhou R, Fen J. J App Phys 2015;118:75902.
[35] Akbudak S, Kushwaha AK. J Phys Chem Solid 2018;115:1–5.
[36] Voigt W. Lehrbuch der Kristallpysik Taubner, Leipzig. 1928. p. 29.
[37] Reuss A, Angew Z. Math Mech 1929;9:49–58.
[38] Hill R. Proc Phys Soc London 1952;65:349.
[39] Pugh SF. Phil Mag Ser 1954;45:823–43.
[40] Benyelloul K, Bouhadda Y, Bououdina M, Faraoun HI, Aourag H, Seddik L. Int J Hydrogen Energy 2014;39:12667–75.
[41] Frantsevich IN, Voronov FF, Bokuta SA, Frantsevich IN. Elastic constants and elastic moduli of metals and insulators handbook. Kiev: Naukova Dumka; 1983. p. 60–180.
[42] Johnston I, Keeler G, Rollins R, Spicklemire S. Solid state physics simulations, the consortium for upper-level physics software. New York: Jhon Wiley; 1996.
[43] Anderson OL. J Phys Chem Solid 1963;24:909–17.
[44] Schreiber E, Anderson OL, Soga N. Elastic constants and their measurements. New York: McGraw-Hill; 1973.
[45] Miao N, Sa B, Zhou J, Sun Z. Comput Mater Sci 2011;50:1559–66.
[46] Li R-Y, Duan Y-H. Phil Mag 2016;96:972–90.
[47] Ranganathan SI, Ostoja-Starzewski M. Phys Rev Lett 2008;101. 055504 1-4.
[48] Marmier A, Lethbridge AD, Walton RI, Smith CW, Parker SC, Evans KE. Comput Phys Commun 2010;181:2102–15.
[49] Surucu G. Mater Chem Phys 2018;203:106.